Nuclear Engineering and Technology 55 (2023) 1585–1590

Contents lists available at ScienceDirect

Nuclear Engineering and Technology

journal homepage: www.elsevier.com/locate/net

Original Article

Impacts of halloysite clay nanoparticles on the structural and γ-ray shielding properties of the epoxy resin

K.G. Mahmoud [a], M.I. Sayyed [b, c, *], S. Hashim [c, **], Aljawhara H. Almuqrin [d], Abu El-Soad A.M [a]

[a] Ural Federal University, St. Mira, 19, 620002, Yekaterinburg, Russia
[b] Department of Physics, Faculty of Science, Isra University, Amman, Jordan
[c] Physics Department, Faculty of Science, Universiti Teknologi Malaysia, 81310, Skudai, Johor, Malaysia
[d] Department of Physics, College of Science, Princess Nourah Bint Abdulrahman University, P.O. Box 84428, Riyadh, 11671, Saudi Arabia

ARTICLE INFO

Article history:
Received 15 November 2022
Received in revised form
12 January 2023
Accepted 9 February 2023
Available online 14 February 2023

Keywords:
Epoxy resin
Halloysite nanoparticles
Monte Carlo simulation
Radiation shielding properties

ABSTRACT

In this study, halloysite nanoparticles-doped epoxy resin was synthesised using the casting method. The MH-300A density metre revealed that the density of the fabricated composites changed from 1.132 to 1.317 g/cm^3 as the halloysite nanoparticle concentration increased. The Fourier transform infrared was recorded for the synthesised composites. Furthermore, the γ-ray shielding properties of the synthesised composites were evaluated using Monte Carlo simulation and a theoretical programme, XCOM. The linear attenuation coefficient of the epoxy resin increased by 43% (at γ-energy of 15 keV) and 14% (at γ-photon energy of 662 keV) when the concentration of the halloysite nanoparticles was increased from 0 wt% to 40 wt%, respectively.

1. Introduction

Halloysite occurs naturally in white clay, and was discovered by Berthier in 1823. It has an average density of 2.5 gcm^{-3} and belongs to the kaolin group of clay minerals. Halloysite is characterised by the presence of many rolled layers, which are formed when clay layers are wrapped around one another under favourable conditions. Halloysite has a chemical composition similar to that of kaolinite; however, in solid halloysite, the two layers are separated by a layer of water molecules [1]. Mineral halloysite is commercially available and reasonably priced. In recent years, nanoparticles within halloysite rocks have gained significant interest, and researchers have investigated the use of halloysite clay minerals for a variety of technical applications, including the delivery of colon cancer medications, the storage of thermal energy, the development of environmental and biosensors, the production of advanced ceramic materials and for the use of plastic fillers as reinforcement materials [2,3]. Several publications have reported the shielding capabilities of various materials, including glass, rocks, ceramics, polymers and alloys due to the prolific use of radiation isotopes in many industries [4–12]. Considering the relative affordability and availability of naturally occurring minerals and rocks, they can be employed as is or as aggregates in producing radiation protection materials [13–15]. Moreover, several studies have been conducted on the protective properties of various rocks, soils, concretes and mineral components [16–19].

Due to their chemical stability, flexibility, low cost, lightweight and ease of production, polymer matrix composites with various fillers have been intensively researched for their potential use as novel radiation shielding materials. Various modifications have been incorporated as fillers in the polymer matrix to create a radiation shield that can be used against X-rays and γ-rays [20–23].

When the fillers of the polymeric matrices are fabricated at the nanoscale, the polymeric composite's optical, electrical, mechanical and physical properties are significantly enhanced. Similarly, incorporating nano-sized fillers in polymeric composites is an effective radiation attenuation technique [24–26]. Nanoparticles can increase the material's capacity to absorb ionising energy since they are more homogenous and exhibit less agglomeration in the composite. Noor Azman et al. [27] examined the effect of WO_3

* Corresponding author. Department of Physics, Faculty of Science, Isra University, Amman, Jordan.
** Corresponding author.
E-mail addresses: dr.mabualssayed@gmail.com (M.I. Sayyed), suhairul@utm.my (S. Hashim).

https://doi.org/10.1016/j.net.2023.02.015

particle dispersed in epoxy on the transmission of X radiation at energies ranging from 25 to 120 keV. They discovered that the effect was more noticeable at lower photon energies. Ran Li et al. studied the radiation shielding characteristics of nano and micro Gd_2O_3 [28] at various loadings distributed in epoxy resin and photon energies of 31–356 keV. They concluded that nano Gd_2O_3 composites were more effective at blocking X and gamma radiations than micro Gd_2O_3 composites. They also discovered that a nano Gd_2O_3 concentration of 5 wt% at 59.53 keV could achieve an enhanced blocking effect of approximately 28%. Mahmoud et al. demonstrated that composites containing PbO nanoparticles are superior to those containing bulk PbO as gamma radiation shielding materials [29]. Literature states that using nanofillers in radiation shielding is feasible; therefore, there is a significant need for additional research into the influence of filler sizes on the gamma radiation shielding features of various epoxy resin composites.

Considering this, the aim of this study is to examine the effect of halloysite nanoparticle weight% on the structural and γ-ray shielding capabilities of epoxy resin composites. Using MCNP code and XCOM theoretical programme, the linear attenuation coefficient of the newly developed epoxy resin reinforced with halloysite nanoparticles was simulated in the 15–2560 keV γ-photon energy interval.

2. Materials and methods

Four halloysite nanoparticles-doped epoxy resins were prepared using the casting method. Commercial epoxy resin and its solidification solution were procured from SlabDOC, while Sigma-Aldrich provided the halloysite nanoparticles. The epoxy resin/solidification solution ratio was maintained at 2/1 for all synthesised samples. The halloysite nanoparticles were added to the epoxy resin/solidification mixture at concentrations of 0 , 10 , 20 and 40 wt %. Each mixture was stirred for 15 min at room temperature before being moulded in a cubic silicon mould with dimensions of 3 cm × 3 cm and varying thicknesses. The moulded samples were allowed to solidify at room temperature for 24 h. The fabricated samples were labelled E-H0, E-H10, E-H20 and E-H40, where H0, H10, H20 and H40 refer to the halloysite nanoparticle concentrations of 0, 10, 20 and 40 wt%, respectively (see Fig. 1).

The Fourier transform infrared (FT–IR) was obtained using PerkinElmer PE 2400 analyser. The FT–IR measurements were performed at wave numbers of 500 cm^{-1} to 3200 cm^{-1}. The MH-300A was utilised to measure the experimental densities of the fabricated E-H composites with an uncertainty of 0.001 g/cm^3.

The linear attenuation coefficient (μ) was simulated using the MCNP transport code in the γ-ray energy range of 15 keV–2506 keV [30]. Generally, an input file is required to complete the MCNP simulation processes. To obtain the MCNP input file, the cell, surface, material, importance, source, tally and cut-off cards are required to be accurately arranged. The arrangement of these cards was discussed in some of our previous publications [31–34]. There are also two important files required for performing the simulation; the nuclear data library is the ENDF/B-VI.8 database in the current study. The output file generated by the programme contains the average track length (ATL) of gamma photons in the current composites along the studied gamma photon energy spectrum. The recorded ATL values were converted to the μ, half-value thickness ($\Delta_{0.5}$) and transmission factor (TF) using the following equations [12,35]:

$$\mu\left(cm^{-1}\right) = \frac{\mathrm{I}}{\mathrm{x}} \ln\left(\frac{I_o}{I_t}\right) \tag{1}$$

The thickness required to absorb half of the applied γ photons is the $\Delta_{0.5}$ and defined in equ. 2 [36,37]:

$$\Delta_{0.5}\ (cm) = \frac{\ln(2)}{\mu} \tag{2}$$

$$TF\ (\%) = \frac{I_t}{I_o} \times 100 \tag{3}$$

3. Results and discussion

The FT–IR spectra of pure epoxy resin (E-H0 sample) and epoxy reinforced by halloysite nanoparticles at various concentrations (E-H10, E-H20 and E-H40 samples) revealed the formation of new bands, as depicted in Fig. 2. One of the previously reported new bands appeared at 913.47 cm^{-1} for samples containing halloysite nanoparticles but disappeared from the pure epoxy E-H0 sample, with the peak intensity increasing as the number of halloysite nanoparticles in the produced composites increases. The peak at 913.47 cm^{-1} is attributed to the inner surface deformation vibration of hydroxyl groups, which occurs at 908 cm^{-1} [38]. The second new band for EH-10, E-H20 and E-H30 appear at 1009 cm^{-1}. These bands could be attributed to the Si–O–Si stretching vibration, which occurs at 1006 cm^{-1} [38]. The band at 1032 cm^{-1} in samples dropped by halloysite nanotubes can be assigned to the stretching mode of apical Si–O occurring at 1105 cm^{-1} [38], whereas, in pure epoxy E-H0, the band represents symmetrical C–O stretching [39].

A partial replacement of epoxy raisin by the halloysite nanoparticle was confirmed in the FTIR-spectra, as previously reported. This partial replacement raises the density (ρ, g/cm^3) of the fabricated composites, as shown in Fig. 3. This increase in the ρ values is due to the substitution of epoxy with lower density (ρ = 1.132 g/cm^3) halloysite nanoparticles (ρ = 2.52 g/cm^3). This substitution raises the ρ values of the fabricated E-H composites from 1.132 to 1.317 g/cm^3 by increasing the halloysite nanoparticle concentration

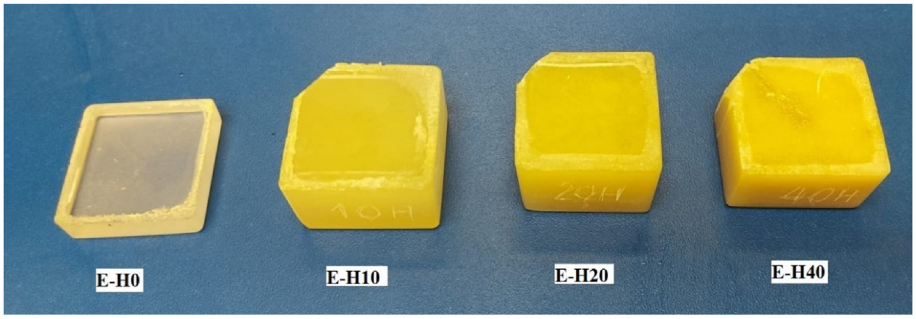

Fig. 1. The fabricated epoxy doped with halloysite nanoparticles.

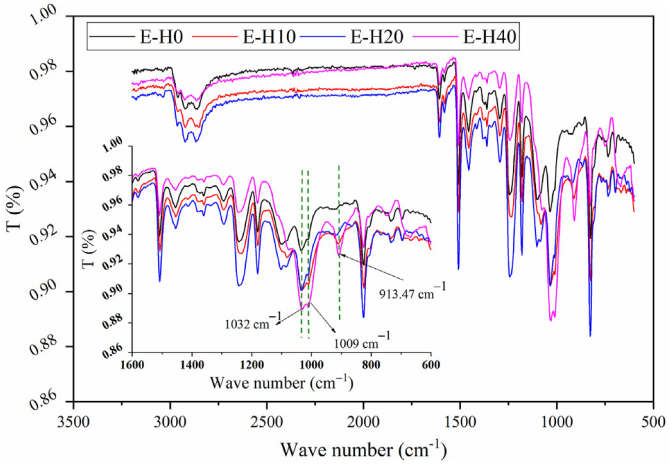

Fig. 2. FT–IR spectra for the synthesised E-H composites.

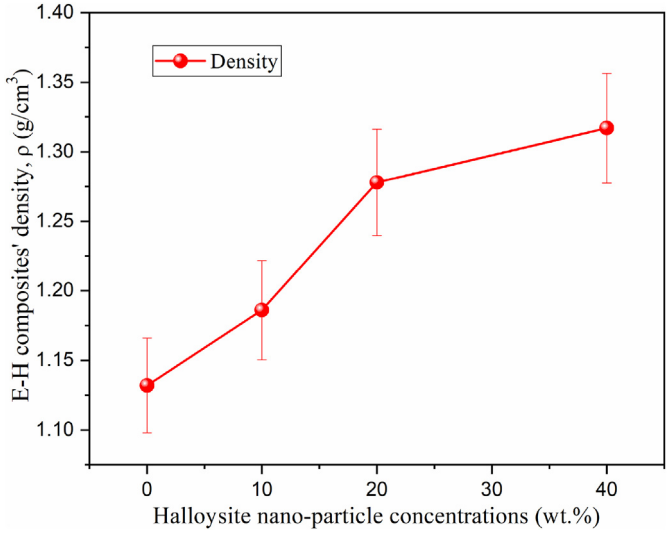

Fig. 3. Variation of the E-H composite densities as a function of the halloysite nanoparticle concentrations.

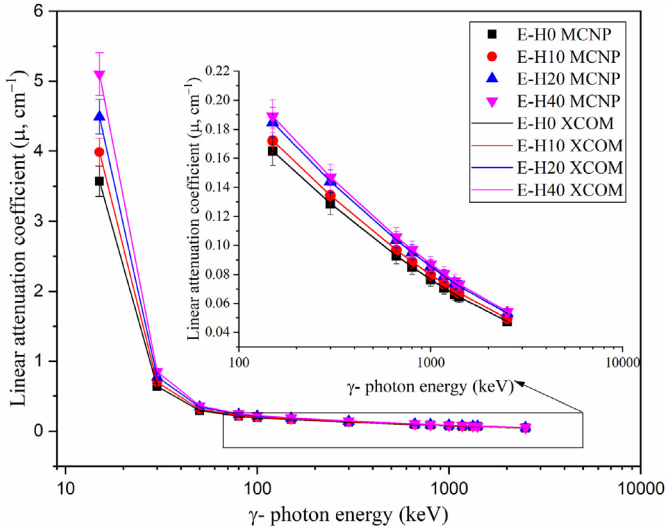

Fig. 4. Variation of the linear attenuation coefficient versus the incident γ-photon energies.

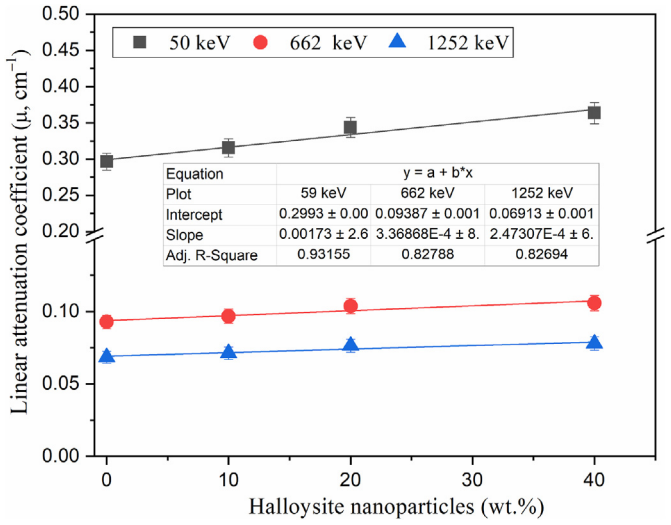

Equation	y = a + b*x		
Plot	59 keV	662 keV	1252 keV
Intercept	0.2993 ± 0.00	0.09387 ± 0.001	0.06913 ± 0.001
Slope	0.00173 ± 2.6	3.36868E-4 ± 8.	2.47307E-4 ± 6.
Adj. R-Square	0.93155	0.82788	0.82694

Fig. 5. Dependence of μ on the halloysite nanoparticle concentrations (wt.%).

from 0 wt% to 40 wt%. Due to the inclusion of halloysite nanoparticles, the density increased, which is essential in understanding the following radiation shielding parameters. The mean track length (MTL) of gamma radiation inside the produced epoxy resin containing halloysite nanoparticles was estimated using the MCNP-5 code. The MTL values were used to calculate the ratio of transmitted photons (I/I_o) that could penetrate the fabricated samples. Following that, a plot of ln (I/I_o) against various thicknesses of the fabricated samples was generated, which aided in determining the LAC for the tested samples. Fig. 4 depicts the linear attenuation coefficient (μ) variations with energy. The simulated and theoretical XCOM μ values are illustrated in the figure. The simulated LAC values were consistent with those estimated by the theoretical software XCOM. The percentage difference between MCS and XCOM data was within the 4% range. The influence of γ-ray interactions steadily diminishes the μ values of any substance. The range of μ values that exhibited downward trends in the current study are 3.568–0.068 cm^{-1} for E-H0, 3.988–0.071 cm^{-1} for E-H10, 4.491–0.076 cm^{-1} for E-H20 and 5.102–0.078 cm^{-1} for E-H40. It can be seen that between 15 and 50 keV, the μ decreased sharply. We discovered that the μ for E-H0 varies from 3.568 to 0.296 cm^{-1}, while those for E-H10, E-H20 and E-H40 vary from 3.988 to 0.316 cm^{-1}, 4.491 to 0.344 cm^{-1} and 5.102 to 0.363 cm^{-1}. This significant variation among these low energies is due to the dominance of the photoelectric effect, which strongly depends on the inverse of the photon's energy (with $1/E^{3.5}$). To elucidate the effect of the halloysite nanoparticles on μ, Fig. 5 was illustrated, depicting the relationship between μ and the halloysite nanoparticles at three energies (50, 662 and 1252 keV). An increase in the concentration of halloysite nanoparticles contributed to an increase in the LAC values of the prepared samples. This increase in the μ is more pronounced at 15 keV than at the other two energies in the same figure. When we calculated the slope of the three lines shown in Fig. 5, we obtained values of 0.0017, 0.00036 and 0.00024 at energies of 50, 662 and 1252 keV, respectively. The μ increased from 3.568 to 5.102 at 15 keV due to changes in the halloysite nanoparticle concentration from 0 wt% to 40 wt%. In other words, pure epoxy resin has lower μ than epoxy resin composites containing 10%, 20% and 40% halloysite nanoparticles. This can be explained using Fig. 3 wherein the densities of the

composites changed linearly with the number of halloysite nanoparticles added to the composites. Therefore, μ increases with density. Thus, we conclude that adding halloysite nanoparticles improves the radiation shielding performance of the prepared composites.

The μ values for the synthesised nano-halloysite doped epoxy E-H composites were compared to those of previously fabricated epoxy-doped Al_2O_3, Fe_2O_3 and a basalt and tungsten mixture [40,41], as shown in Fig. 6. The synthesised composites E-H-20 and E-H40 yielded μ values of 0.104 and 0.106 cm^{-1}, respectively, higher than the μ values recorded for epoxy/6% Al_2O_3, epoxy/15% Al_2O_3, epoxy/6% Fe_2O_3, epoxy/15% Fe_2O_3 and epoxy/Pb_3O_4. However, BET-0, BET-5.9, BET-15.3, BET-24.6 and BET-33.1 samples with mixed basalt and tungsten concentrations of 0%, 5.9%, 15.3%, 24.6% and 33.1% have μ values higher than those of the synthesised samples. The dense doping tungsten element (W with a density of 19.25 g/cm^3) is responsible for the high μ values of the BET composites.

We also investigated the $\Delta_{0.5}$ for the newly developed composites, and in Fig. 7, we will discuss the effect of photon energy on the $\Delta_{0.5}$. Using the same figure, we can also study the relationship between $\Delta_{0.5}$ and the concentration of halloysite nanoparticles. First, $\Delta_{0.5}$ has a positive relationship with the radiation energy. At 15 keV, the $\Delta_{0.5}$ is very small (in the range of 0.14–0.19 cm), indicating that an effective shield requires a layer of the prepared composite with a thickness of less than 0.2 cm. When we considered the energy of 30 keV, we discovered that a layer with a thickness of 0.82–1.09 cm is required to perform the same task. However, at the same energy (i.e. 30 keV), the composite containing 10%–40% halloysite nanoparticles has a $\Delta_{0.5}$ ranging from 0.82 to 0.99 cm (still less than 1 cm). Furthermore, when we examined the energy of 50 keV, we discovered that $\Delta_{0.5}$ is greater than 1 cm and less than 3 cm (varying between 1.91 and 2.34 cm). Thus, we can conclude that a 2.5 cm layer of any composition in this work can effectively shield radiation with E ≤ 50 keV. We discovered that as the energy increases beyond 100 keV, the $\Delta_{0.5}$ increases and exceeds 3.5 cm, specifically for pure epoxy. At 800 keV, we discovered that the layer of the prepared composites must be 7.14–8.13 cm thick to attenuate 50% of the incoming radiation. The $\Delta_{0.5}$ reaches maximum values of 14.63, 14.02, 13.08 and 12.81 cm for E-H0, E-H10, E-H20 and E-H40 at a higher energy of 2506 keV, respectively.

To understand the effect of adding halloysite nanoparticles to the epoxy resin into the $\Delta_{0.5}$, we examined the data in Fig. 7 and

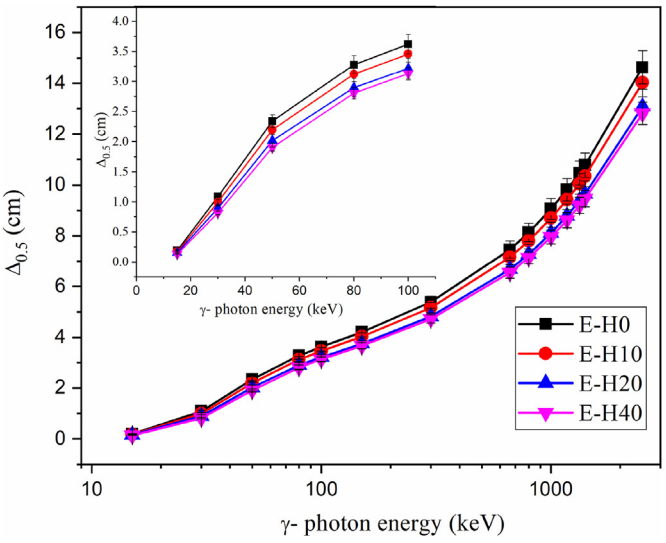

Fig. 7. Influence of the incoming γ-photon energy on the $\Delta_{0.5}$ values for the fabricated E-H composites.

discovered that the $\Delta_{0.5}$ follows the order E-H0 > E-H10 > E-H20 > E-H40. This indicates that the incorporation of halloysite nanoparticles into pure epoxy resin resulted in a decrease in HVL. This is ascribed to the increased density of the composites due to adding the halloysite nanoparticles. As a result of the inverse relationship between density and HVL, as density increases, the HVL decreases. This is consistent with previous findings for other materials, such as alloys and glass [42–44].

We plotted the relationship between $\Delta_{0.5}$ and λ (mean free path) and the density of the composites in Fig. 8. This data is exhibited only at 662 keV. Both parameters decreased with increasing composite thickness, which is logical given the high probability of photon interaction with a dense medium.

In Fig. 9, we investigated the TF (I/I_o) as a function of energy. It should be noted that the TF is very low at 15 keV (2.82% for E-H0, 1.85% for E-H10, 1.12% for E-H20 and 0.61% for E-H40), implying that all prepared composites can attenuate nearly all 15 keV radiations. Thus, these newly developed composites have a high potential for use in low-energy radiation shielding applications. However, the TF

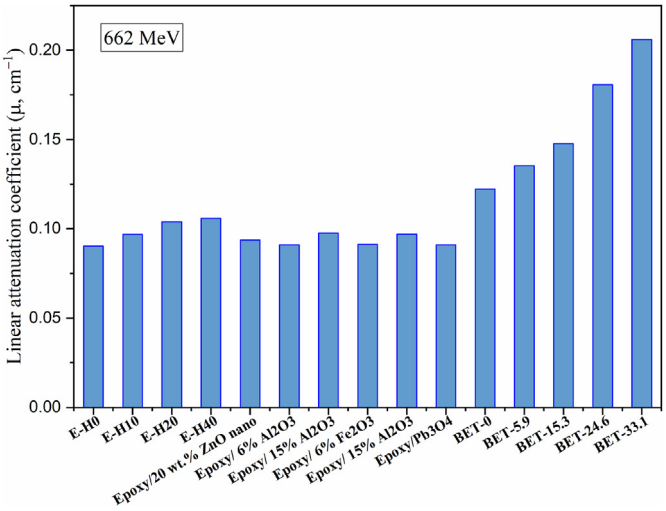

Fig. 6. Comparison between the μ of the fabricated E-H composites with some similar reported polymers.

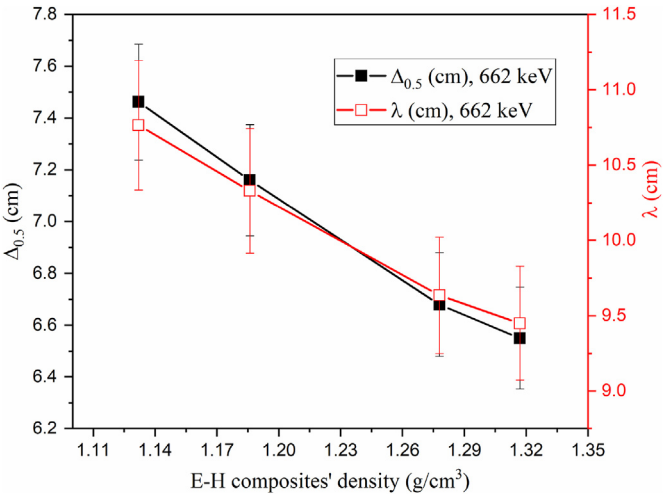

Fig. 8. Impacts of the halloysite nanoparticle concentrations on the $\Delta_{0.5}$ values for the fabricated E-H composites.

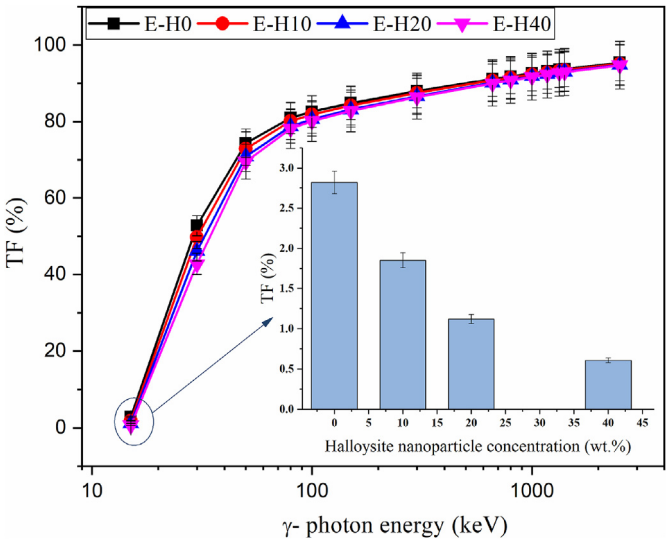

Fig. 9. Variation of the E-H composite transmission values (TF, %) versus the incoming γ-photon energies.

at 30 keV attenuated approximately 42.75%–52.80% of the radiations, implying that the radiation shielding performance of the composites is weaker than at 15 keV. This range (42.75%–52.80%) implies that the newly developed composites can attenuate approximately half of the incoming radiation with energy of 30 keV. To summarise, as the energy changes from 15 to 30 keV, the TF increases, and thus the attenuation performance decreases. When we examine the TF for energies greater than 30 keV, we find that the TF increases to approximately 69.75%–74.35%when E = 50 keV. This means that the composite can only attenuate approximately 30% of the photons, whereas 70% of the radiation at 50 keV can easily penetrate the prepared composites. We discovered that the TF is greater than 90% for E > 66 keV, implying that these composites can only attenuate 10% of the radiation and are therefore unsuitable for radiation shielding applications. As a result, we attempt to investigate the effect of increasing the thickness of these composites on the TF. In Fig. 10, we investigated six different thicknesses for each composition and calculated the TF at 662 keV

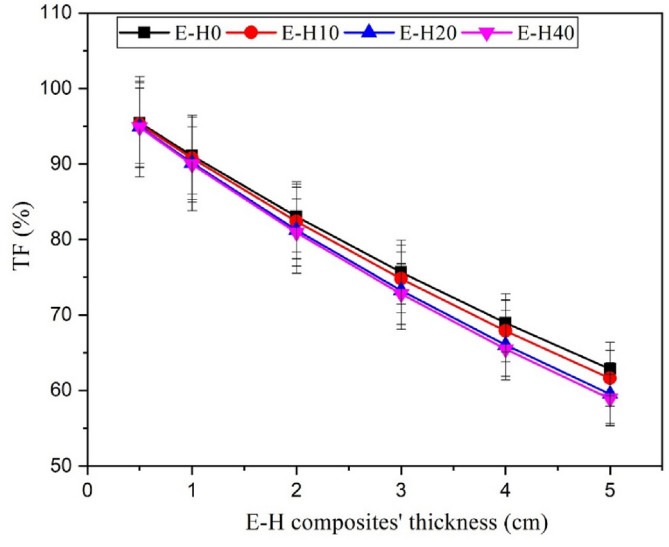

Fig. 10. Impacts of the fabricated E-H composite thicknesses on the TF values.

for each sample. Due to the change in thickness from 0.5 to 5 cm, the TF for E-H0 decreased from 95.46% to 62.85%. Therefore, increasing the thickness of these compositions is one effective way of improving their shielding performances. We discovered that increasing the thickness of H-E10 improved attenuation performance, with the TF for this sample decreasing from 95.27% to 61.63%. The TF for H-E20 reduced from 94.94% to 59.52%.

4. Conclusion

Four halloysite nanoparticle-based epoxy resin composites were fabricated at room temperature to evaluate the effects of halloysite nanoparticles on the structural and γ-ray shielding properties of the epoxy resin. The FT–IR spectra revealed that reinforcing epoxy resin with halloysite nanoparticles results in the formation of new bands at 913.47 cm^{-1}, 1009 cm^{-1} and 1032 cm^{-1} due to deformation vibration of the inner surface of the hydroxyl groups, stretching vibration of Si–O–Si and stretching mode of apical Si–O, respectively. Furthermore, the experimental measurements of the densities of the composites show an increase from 1.132 g/cm^3 to 1.317 g/cm^3 by increasing the halloysite nanoparticle concentration from 0 wt% to 40 wt%. Furthermore, MCNP revealed that the addition of halloysite nanoparticles increases the linear attenuation coefficient of the fabricated composites by 43% (for gamma energy of 15 keV), 17% (for gamma energy of 662 keV) and 17% (for gamma energy of 1252 keV) when the halloysite nanoparticle concentration increased from 0 wt% to 40 wt%. The increase in the linear attenuation coefficient of the synthesised composites has a greater impact on the rest of the shielding properties, where $\Delta_{0.5}$ and TF values reduced as the halloysite nanoparticle concentrations increased. As a result, the current study concluded that the shielding properties of the fabricated composites were improved against low and intermediate gamma photon energies.

Declaration of competing interest

The authors declare that they have no known competing financial interests or personal relationships that could have appeared to influence the work reported in this paper.

Acknowledgements

The authors express their gratitude to the Princess Nourah bint Abdulrahman University Researchers Supporting Project number (PNURSP2023R2), Princess Nourah bint Abdulrahman University, Riyadh, Saudi Arabia. M. I. Sayyed and S. Hashim gratefully acknowledge Universiti Teknologi Malaysia for providing Prominent Visiting Researcher Scheme (RJ3000.7113.3F000) under the Department Deputy of Vice-Chancellor (Research and Innovation) initiatives.

References

[1] P. Yuan, D. Tan, F. Annabi-Bergaya, Properties and applications of halloysite nanotubes: recent research advances and future prospects, Appl. Clay Sci. 112–113 (2015) 75–93, https://doi.org/10.1016/j.clay.2015.05.001.
[2] S.A. Konnova, I.R. Sharipova, T.A. Demina, Y.N. Osin, D.R. Yarullina, O.N. Ilinskaya, Y.M. Lvov, R.F. Fakhrullin, Biomimetic cell-mediated three-dimensional assembly of halloysite nanotubes, Chem. Commun. 49 (2013) 4208–4210, https://doi.org/10.1039/C2CC38254G.
[3] K.A.M.Ş.E. E.G Kovaleva, A.M. AbuEl-soad, M.I. Sayyed, Modified halloysite minerals for radiation shielding purposes, J Radiat Res Appl Sci (2020), https://doi.org/10.1080/16878507.2019.1699680.
[4] H.S. Gökçe, B.C. Öztürk, N.F. Çam, Ö. Andiç-Çakır, Gamma-ray attenuation coefficients and transmission thickness of high consistency heavyweight concrete containing mineral admixture, Cem. Concr. Compos. 92 (2018) 56–69, https://doi.org/10.1016/j.cemconcomp.2018.05.015.
[5] S. Kaewjaeng, S. Kothan, W. Chaiphaksa, N. Chanthima, R. Rajaramakrishna,

H.J. Kim, J. Kaewkhao, High transparency La2O3-CaO-B2O3-SiO2 glass for diagnosis x-rays shielding material application, Radiat. Phys. Chem. 160 (2019) 41–47, https://doi.org/10.1016/j.radphyschem.2019.03.018.
[6] Bünyamin Aygün,"Neutron and gamma radiation shielding Ni based new type super alloys development and production by Monte Carlo Simulation technique, Radiation Physics and Chemistry 188 (2021) 109630.
[7] K.A. Naseer, G. Sathiyapriya, K. Marimuthu, T. Piotrowski, M.S. Alqahtani, E.S. Yousef, Optical, elastic, and neutron shielding studies of Nb2O5 varied Dy3+ doped barium-borate glasses, Optik (Stuttg) 251 (2022) 168436, https://doi.org/10.1016/j.ijleo.2021.168436.
[8] B. Aygün, High alloyed new stainless steel shielding material for gamma and fast neutron radiation, Nucl. Eng. Technol. 52 (2020) 647–653, https://doi.org/10.1016/j.net.2019.08.017.
[9] M. Dong, X. Xue, H. Yang, D. Liu, C. Wang, Z. Li, A novel comprehensive sutilisation of vanadium slag: as gamma ray shielding material, J. Hazard Mater. 318 (2016) 751–757, https://doi.org/10.1016/j.jhazmat.2016.06.012.
[10] M. Dong, X. Xue, A. Kumar, H. Yang, M.I. Sayyed, S. Liu, E. Bu, A novel method of sutilisation of hot dip sgalvanising slag using the heat waste from itself for protection from radiation, J. Hazard Mater. 344 (2018) 602–614, https://doi.org/10.1016/j.jhazmat.2017.10.066.
[11] K.A. Naseer, K. Marimuthu, K.A. Mahmoud, M.I. Sayyed, Impact of Bi2O3 modifier concentration on barium–zincborate glasses: physical, structural, elastic, and radiation-shielding properties, The European Physical Journal Plus 136 (2021) 116, https://doi.org/10.1140/epjp/s13360-020-01056-6.
[12] K.A. Naseer, K. Marimuthu, K.A. Mahmoud, M.I. Sayyed, The concentration impact of Yb3+ on the bismuth boro-phosphate glasses: physical, structural, optical, elastic, and radiation-shielding properties, Radiat. Phys. Chem. 188 (2021), 109617, https://doi.org/10.1016/j.radphyschem.2021.109617.
[13] S.S. Obaid, D.K. Gaikwad, P.P. Pawar, Determination of gamma ray shielding parameters of rocks and concrete, Radiat. Phys. Chem. 144 (2018) 356–360, https://doi.org/10.1016/j.radphyschem.2017.09.022.
[14] A.T. Şensoy, H.S. Gökçe, Simulation and soptimisation of gamma-ray linear attenuation coefficients of barite concrete shields, Construct. Build. Mater. 253 (2020), 119218, https://doi.org/10.1016/j.conbuildmat.2020.119218.
[15] K.A. Mahmoud, O.L. Tashlykov, A.F. el Wakil, H.M.H. Zakaly, I.E. el Aassy, Investigation of radiation shielding properties for some building materials reinforced by basalt powder investigation of radiation shielding properties for some building materials reinforced by basalt powder, AIP Conf. Proc. (2019), 020036.
[16] A.M. Zeyad, I.Y. Hakeem, M. Amin, B.A. Tayeh, I.S. Agwa, Effect of aggregate and fibre types on ultra-high-performance concrete designed for radiation shielding, J. Build. Eng. 58 (2022), 104960, https://doi.org/10.1016/j.jobe.2022.104960.
[17] L. Luo, Z. Chen, Q. Tao, L. Xie, D. Jin, Z. Li, D. Deng, Effects of high temperatures on the splitting tensile strength and gamma ray shielding performance of radiation shielding concrete, Construct. Build. Mater. 343 (2022), 127953, https://doi.org/10.1016/j.conbuildmat.2022.127953.
[18] A.M. Zayed, M.A. Masoud, M.G. Shahien, H.S. Gökçe, K. Sakr, W.A. Kansouh, A.M. El-Khayatt, Physical, mechanical, and radiation attenuation properties of serpentine concrete containing boric acid, Construct. Build. Mater. 272 (2021), 121641, https://doi.org/10.1016/j.conbuildmat.2020.121641.
[19] S. Arivazhagan, K.A. Naseer, K.A. Mahmoud, K.V. Arun Kumar, N.K. Libeesh, M.I. Sayyed, M.S. Alqahtani, E.S. Yousef, M.U. Khandaker, Gamma-ray protection capacity evaluation and satellite data based mapping for the limestone, charnockite, and gneiss rocks in the Sirugudi taluk of the Dindigul district, India, Radiat. Phys. Chem. 196 (2022), 110108, https://doi.org/10.1016/j.radphyschem.2022.110108.
[20] M. Yilmaz, M.E. Pekdemir, E. Özen Öner, Evaluation of Pb doped Poly(lactic acid) (PLA)/Poly(ethylene glycol) (PEG) blend composites regarding physicochemical and radiation shielding properties, Radiat. Phys. Chem. 202 (2023), 110509, https://doi.org/10.1016/j.radphyschem.2022.110509.
[21] P. Wang, X. Tang, H. Chai, D. Chen, Y. Qiu, Design, fabrication, and properties of a continuous carbon-fiber reinforced Sm 2 O 3/polyimide gamma ray/neutron shielding material, Fusion Eng. Des. 101 (2015) 218–225, https://doi.org/10.1016/j.fusengdes.2015.09.007.
[22] V. Harish, N. Nagaiah, T.N. Prabhu, K.T. Varughese, Preparation and scharacterisation of lead monoxide filled unsaturated polyester based polymer composites for gamma radiation shielding applications, J. Appl. Polym. Sci. 112 (2009) 1503–1508, https://doi.org/10.1002/app.29633.
[23] M. Dong, X. Xue, H. Yang, Z. Li, Highly cost-effective shielding composite made from vanadium slag and boron-rich slag and its properties, Radiat. Phys. Chem. 141 (2017) 239–244, https://doi.org/10.1016/j.radphyschem.2017.07.023.
[24] S.A. Gursal, N. Mehboob, B. Ahmed, M.S. Mehmood, On the neutron shielding efficacy of flexible silicone infused with CdO nanoparticles, Radiat. Phys. Chem. 202 (2023), 110555, https://doi.org/10.1016/j.radphyschem.2022.110555.
[25] S. Kim, Y. Ahn, S.H. Song, D. Lee, Tungsten nanoparticle anchoring on boron nitride nanosheet-based polymer nanocomposites for complex radiation shielding, Compos. Sci. Technol. 221 (2022), 109353, https://doi.org/10.1016/j.compscitech.2022.109353.
[26] G.A.M. Amin, M.H. Abd-El Salam, Optical, dielectric and electrical properties of PVA doped with Sn nanoparticles, Mater. Res. Express 1 (2014), 025024, https://doi.org/10.1088/2053-1591/1/2/025024.
[27] N.Z. Noor Azman, S.A. Siddiqui, R. Hart, I.M. Low, Effect of particle size, filler loadings and x-ray tube voltage on the transmitted x-ray transmission in tungsten oxide—epoxy composites, Appl. Radiat. Isot. 71 (2013) 62–67, https://doi.org/10.1016/j.apradiso.2012.09.012.
[28] R. Li, Y. Gu, Y. Wang, Z. Yang, M. Li, Z. Zhang, Effect of particle size on gamma radiation shielding property of gadolinium oxide dispersed epoxy resin matrix composite, Mater. Res. Express 4 (2017), 035035, https://doi.org/10.1088/2053-1591/aa6651.
[29] M.E. Mahmoud, A.M. El-Khatib, M.S. Badawi, A.R. Rashad, R.M. El-Sharkawy, A.A. Thabet, Fabrication, scharacterisation and gamma rays shielding properties of nano and micro lead oxide-dispersed-high density polyethylene composites, Radiat. Phys. Chem. 145 (2018) 160–173, https://doi.org/10.1016/j.radphyschem.2017.10.017.
[30] X-5 Monte Carlo Team, MCNP — A General Monte Carlo N-Particle Transport Code, 2003. Version 5, La-Ur-03-1987. II.
[31] M.I. Sayyed, E. Hannachi, K.A. Mahmoud, Y. Slimani, Synthesis of different (RE) BaCuO ceramics, study their structural properties, and tracking their radiation protection efficiency using Monte Carlo simulation, Mater. Chem. Phys. 276 (2022), 125412, https://doi.org/10.1016/j.matchemphys.2021.125412.
[32] M.I. Sayyed, M.Y. Hanfi, K.A. Mahmoud, A. Abdelaziem, Theoretical Investigation of the radiation-protection properties of the CBS glass family, Optik 258 (2022), 168851, https://doi.org/10.1016/j.ijleo.2022.168851.
[33] E. Hannachi, K.A. Mahmoud, M.I. Sayyed, Y. Slimani, Effect of sintering conditions on the radiation shielding characteristics of YBCO superconducting ceramics, J. Phys. Chem. Solid. 164 (2022), 110627, https://doi.org/10.1016/j.jpcs.2022.110627.
[34] E. Hannachi, M.I. Sayyed, A.H. Almuqrin, K.G. Mahmoud, Study of the structure and radiation-protective properties of yttrium barium copper oxide ceramic doped with different oxides, J. Alloys Compd. 885 (2021), 161142, https://doi.org/10.1016/j.jallcom.2021.161142.
[35] P. Evangelin Teresa, K.A. Naseer, K. Marimuthu, H. Alavian, M.I. Sayyed, Influence of modifiers on the physical, structural, elastic and radiation shielding competence of Dy3+ ions doped Alkali boro-tellurite glasses, Radiat. Phys. Chem. 189 (2021), 109741, https://doi.org/10.1016/j.radphyschem.2021.109741.
[36] A.S. Abouhaswa, M.I. Sayyed, K.A. Mahmoud, Y. Al-Hadeethi, Direct influence of mercury oxide on structural, optical and radiation shielding properties of a new borate glass system, Ceram. Int. 46 (2020) 17978–17986, https://doi.org/10.1016/j.ceramint.2020.04.112.
[37] M.I. Sayyed, M.H.M. Zaid, N. Effendy, K.A. Matori, H.A.A. Sidek, E. Lacomme, K.A. Mahmoud, M.M. AlShammari, The influence of PbO and Bi2O3 on the radiation shielding and elastic features for different glasses, J. Mater. Res. Technol. 9 (2020) 8429–8438, https://doi.org/10.1016/j.jmrt.2020.05.113.
[38] P. Luo, Y. Zhao, B. Zhang, J. Liu, Y. Yang, J. Liu, Study on the adsorption of Neutral Red from aqueous solution onto halloysite nanotubes, Water Res. 44 (2010) 1489–1497, https://doi.org/10.1016/j.watres.2009.10.042.
[39] P. Maity, S.v. Kasisomayajula, V. Parameswaran, S. Basu, N. Gupta, Improvement in surface degradation properties of polymer composites due to preprocessed nanometric alumina fillers, IEEE Trans. Dielectr. Electr. Insul. 15 (2008) 63–72, https://doi.org/10.1109/T-DEI.2008.4446737.
[40] M.J.R. Aldhuhaibat, M.S. Amana, N.J. Jubier, A.A. Salim, Improved gamma radiation shielding traits of epoxy composites: evaluation of mass attenuation coefficient, effective atomic and electron number, Radiat. Phys. Chem. 179 (2021), 109183, https://doi.org/10.1016/j.radphyschem.2020.109183.
[41] Y. Hou, M. Li, Y. Gu, Z. Yang, R. Li, Z. Zhang, Gamma ray shielding property of tungsten powder modified continuous basalt fiber reinforced epoxy matrix composites, Polym. Compos. 39 (2018) E2106, https://doi.org/10.1002/pc.24469. –E2115.
[42] Aljawhara H. Almuqrin, M. I. Sayyed, Radiation shielding characterizations and investigation of TeO2–WO3–Bi2O3 and TeO2–WO3–PbO glasses, Applied Physics A (2021) 127:190.
[43] I.S. Mahmoud, Shams A.M. Issa, Yasser B. Saddeek, H.O. Tekin, Ozge Kilicoglu, T. Alharbi, M.I. Sayyed, T.T. Erguzel, Reda Elsaman,Gamma, neutron shielding and mechanical parameters for lead vanadate glasses, Ceramics International 45 (2019) 14058–14072.
[44] Y. Al-Hadeethi, M.I. Sayyed, Radiation attenuation properties of Bi2O3–Na2O– V2O5– TiO2–TeO2 glass system using Phy-X / PSD software, Ceramics international 46 (2020) 4795–4800.